Journal of Advanced Ceramics
2022, **11**(4): 532–544
https://doi.org/10.1007/s40145-021-0553-3
ISSN 2226-4108
CN 10-1154/TQ

Research Article

Texture and anisotropy of hot-pressed h-BN matrix composite ceramics with *in situ* formed YAG

Zhuo ZHANG[a,b], Xiaoming DUAN[a,b,c,*], Zhuo TIAN[d], Yujin WANG[a,b,*], Lan WANG[a,b], Lei CHEN[a,b], Baofu QIU[a,b], Delong CAI[a,b], Peigang HE[a,b], Dechang JIA[a,b,c,*], Yu ZHOU[a,b]

[a]*Key Laboratory of Advanced Structural-Functional Integration Materials & Green Manufacturing Technology*, *Harbin Institute of Technology*, *Harbin 150001*, *China*
[b]*Institute for Advanced Ceramics*, *School of Materials Science and Engineering*, *Harbin Institute of Technology*, *Harbin 150001*, *China*
[c]*State Key Laboratory of Advanced Welding and Joining*, *Harbin Institute of Technology*, *Harbin 150001*, *China*
[d]*School of Electromechanical Engineering*, *Guangdong University of Technology*, *Guangzhou 510006*, *China*

Received: August 22, 2021; Revised: October 17, 2021; Accepted: November 9, 2021

Abstract: Textured hexagonal boron nitride (h-BN) matrix composite ceramics were prepared by hot-pressing using different contents of $3Y_2O_3$–$5Al_2O_3$ (molar ratio of 3:5) as the sintering additive. During hot-pressing, the liquid $Y_3Al_5O_{12}$ (YAG) phase showing good wettability to h-BN grains was *in situ* formed through the reaction between Y_2O_3 and Al_2O_3, and a coherent relationship between h-BN and YAG was observed with $[010]_{h\text{-}BN}//[\bar{1}11]_{YAG}$ and $(002)_{h\text{-}BN}//(321)_{YAG}$. In the YAG liquid phase environment formed during hot-pressing, plate-like h-BN grains were rotated under the uniaxial sintering pressure and preferentially oriented with their basal surfaces perpendicular to the sintering pressure direction, forming textured microstructures with the *c*-axis of h-BN grains oriented parallel to the sintering pressure direction, which give these composite ceramics anisotropy in their mechanical and thermal properties. The highest texture degree was found in the specimen with 30 wt% YAG, which also possesses the highest anisotropy degree in thermal conductivity. The aggregation of YAG phase was observed in the specimen with 40 wt% YAG, which resulted in the buckling of h-BN plates and significantly reduced the texture degree.

Keywords: hexagonal boron nitride (h-BN); liquid phase sintering; texture; anisotropy

1 Introduction

Hexagonal boron nitride (h-BN) has a layered structure similar to that of graphite, where B and N atoms are combined by covalent bonds with sp^2 hybridization in the same atomic layer, while different atomic layers are combined by van der Waals (vdW) forces [1–4]. Such a structure gives single h-BN crystal anisotropic physical properties. Its elastic moduli along the *a*- and *b*-axis, and the *c*-axis were calculated to be 837.99 and 33.40 GPa, respectively [5,6], giving textured h-BN ceramics with preferentially oriented grain anisotropic mechanical properties [7]. Its thermal conductivity

* Corresponding authors.
E-mail: X. Duan, duanxiaoming@hit.edu.cn, dxmhit@126.com;
Y. Wang, wangyuj@hit.edu.cn;
D. Jia, dcjia@hit.edu.cn

along the *a*- and *b*-axis, and the *c*-axis was calculated to be 4.1 and 537 W/(m·K), respectively [8], together with its insulating property [9], making h-BN matrix composites the promising thermal management devices in electronics [10–15].

The strong sp^2 covalent bonds combining B and N atoms result in a low atomic diffusion rate even at high sintering temperatures, and the plate-like shape of h-BN grains usually form the "house of cards" structure with high porosity, making h-BN ceramics hard to be densified during sintering [16–19]. Introducing sintering additives composed of two or more oxides which can form liquid phases at high sintering temperatures and fill these pores between plate-like h-BN grains, such as Y_2O_3–Al_2O_3, Y_2O_3–SiO_2, Yb_2O_3–MgO, Yb–Si–Al(N)–O, and La–Al–Si–O [20–26], has been proven to be an effective method to improve the sinterability of h-BN ceramics.

Compared with plate-like h-BN powders with large grain sizes, fine h-BN powders with more defects are easier to be densified due to their high specific surface area and defect energy [27,28]. However, the final gain size of h-BN ceramics prepared from fine h-BN powders is limited even with sintering additives which can form liquid phases during sintering [29–31], and thus h-BN ceramics with highly textured microstructures cannot be obtained. Plate-like h-BN powders with larger grain sizes and sintering additives which can form liquid phases are necessary for the fabrication of textured h-BN matrix composite ceramics with significant anisotropy.

In our previous study, the textured h-BN matrix composite specimen with an index of orientation preference (IOP) of −530 was prepared by hot-pressing using 20 wt% $3Y_2O_3$–$5Al_2O_3$ with a molar ratio of 3:5 as the sintering additive, which was transformed into YAG phase showing good wettability to h-BN grains [22]. In this study, different contents (10, 20, 30, and 40 wt%) of $3Y_2O_3$–$5Al_2O_3$ were introduced to prepare h-BN matrix composite ceramics by hot-pressing to investigate the influence of YAG contents on the texture and anisotropy in the mechanical and thermal properties of the composite ceramics.

2 Materials and methods

The raw materials were h-BN powders with a platelike morphology (~15 μm in diameter and ~0.3 μm in thickness, purity > 99%), Al_2O_3 powders (~0.2 μm, purity > 99.9%), and Y_2O_3 powders (~2 μm, purity > 99.9%). $3Y_2O_3$–$5Al_2O_3$ (molar ratio of 3:5) were used as the sintering additive. Four specimens, whose mass ratios of h-BN to the sintering additive were set as 9:1, 8:2, 7:3, and 6:4, were prepared as follows: Raw powders were mixed using Al_2O_3 balls in ethanol on a pot-mill machine with a rotation speed of 80 rpm for 24 h and then dried on a hot plate set at 70 ℃, and then the mixed powders were loaded into a *Φ*50 mm cylindrical graphite die and hot-pressed at 1900 ℃ under a uniaxial pressure of 30 MPa in N_2 atmosphere for 1 h. Hot-pressed h-BN matrix composite ceramics with 10 wt%, 20 wt%, 30 wt%, and 40 wt% YAG (it will be proven in Section 3.1 that Y_2O_3 and Al_2O_3 fully reacted during hot-pressing, forming YAG with a cubic crystal structure) were marked as BN-1YAG, BN-2YAG, BN-3YAG, and BN-4YAG, respectively.

Bulk densities of the hot-pressed specimens were measured by Archimedes method. Phase compositions and crystallographic orientation were analyzed by the X-ray diffractometer (XRD; X′PERT, Panalytical, the Netherlands). Further analyses on phases and interface microstructure were realized by the transmission electron microscope (TEM; Tecnai G2 F30, FEI, USA). Properties were measured along three different loading directions by the electronic universal testing machine (Model 5569, Instron, USA). The flexural strength was tested on the 3 mm × 4 mm × 36 mm sample bars by three-point bending with a span of 30 mm and a crosshead speed of 0.5 mm/min; the elastic moduli were tested using strain gauges stuck on the tensile surfaces of sample bars used for strength testing; the fracture toughness was tested on 2 mm × 4 mm × 20 mm single-edge-notched beams with a span of 16 mm and a crosshead speed of 0.05 mm/min. Fracture morphologies were observed using the scanning electron microscope (SEM; Quanta 200 FEG, FEI, USA). Coefficients of thermal expansion (CTEs) were measured on 5 mm × 5 mm × 25 mm bars using a dilatometer (DTL 402C, Netzsch, Germany). Specific heat capacity and thermal diffusivity were measured on *Φ*12.7 mm × (2–3) mm discs by a laser flash apparatus (LFA 427, Netzsch, Germany) and the thermal conductivity was calculated from the specific heat capacity and thermal diffusivity.

3 Results and discussion

3.1 Phase compositions, texture, and interface microstructure

Figure 1 shows the XRD patterns measured on both

top surface (TS) perpendicular to the sintering pressure direction and side surface (SS) parallel to the sintering pressure direction of h-BN matrix composite ceramics hot-pressed using different contents of $3Y_2O_3$–$5Al_2O_3$ additive. All specimens are composed of two phases: h-BN and YAG, indicating that Y_2O_3 and Al_2O_3 with the molar ratio of 3:5 have fully reacted. They all show a much higher h-BN(002) diffraction peak for TS than that for SS and a higher h-BN(100) diffraction peak for SS than that for TS, which can be seen in the illustrations showing the complete (002) diffraction peaks at the top-right side of these XRD patterns in Fig. 1, indicating that all specimens possess highly textured microstructures with the *c*-axis of h-BN grains preferentially oriented parallel to the sintering pressure direction, which were attributed to the rotation of plate-like h-BN grains under the uniaxial sintering pressure in the YAG liquid phase environment.

Figure 2 gives the relative densities, IOP, and Lotgering orientation factors f_{00l} of hot-pressed h-BN matrix composite ceramics with different YAG contents. The relative density increases with the increase of the YAG content and reaches the highest for BN-4YAG (92.36%), as the liquid YAG phase formed during hot-pressing acted as the pore filler between plate-like h-BN grains.

IOP and f_{00l} are used to quantitively characterize the texture degree of h-BN matrix composite ceramics. IOP was calculated according to Eq. (1) [32]:

$$\mathrm{IOP} = \begin{cases} \dfrac{(I_{100}/I_{002})\mathrm{TS}}{(I'_{100}/I'_{002})\mathrm{SS}}, & (I_{100}/I_{002})\mathrm{TS} > (I'_{100}/I'_{002})\mathrm{SS} \\ -\dfrac{(I'_{100}/I'_{002})\mathrm{SS}}{(I_{100}/I_{002})\mathrm{TS}}, & (I_{100}/I_{002})\mathrm{TS} < (I'_{100}/I'_{002})\mathrm{SS} \end{cases} \quad (1)$$

where I_{hkl} and I'_{hkl} are the intensities of (*hkl*) diffraction peaks for TS and SS, respectively. For a hot-pressed h-BN matrix composite specimen, IOP = ±1 indicates that it consists of randomly oriented h-BN grains; IOP < −1 and IOP > 1 indicate that its h-BN grains are preferentially oriented with the *c*-axis parallel and perpendicular to the uniaxial sintering pressure direction, respectively. In this study, a negative IOP with a larger absolute value indicates a higher texture degree.

The f_{00l} was calculated according to Eqs. (2) and (3) [33]:

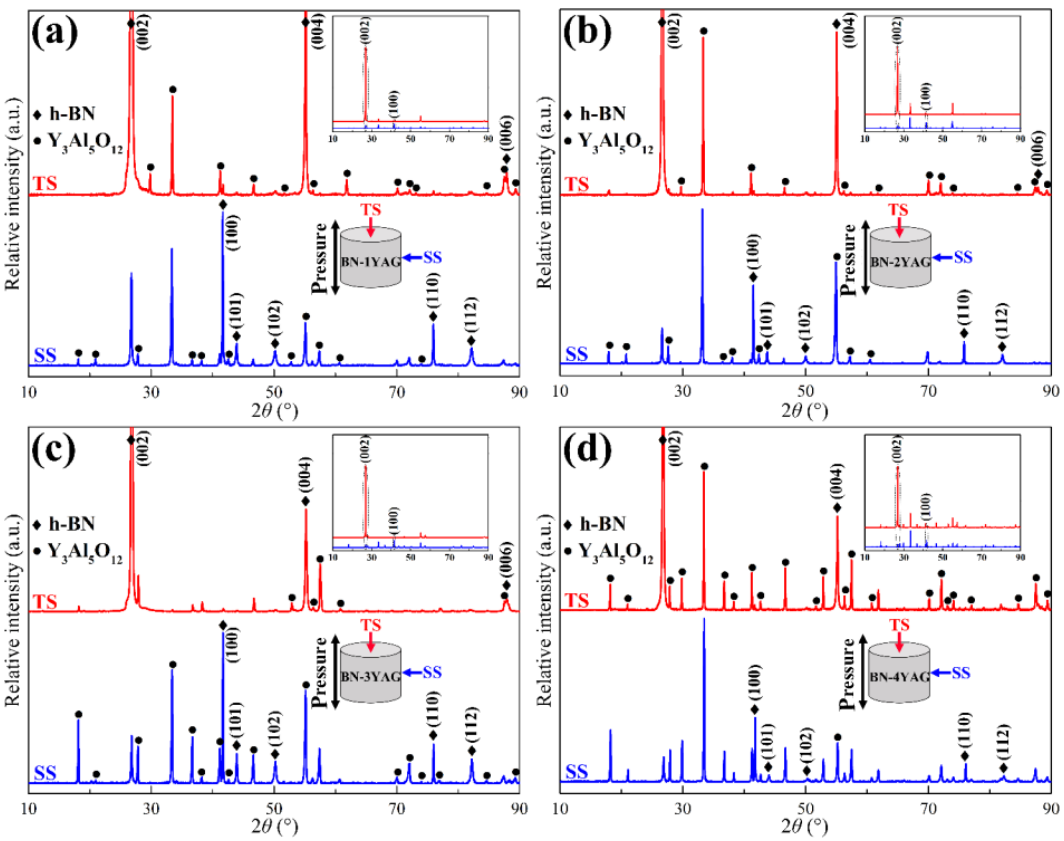

Fig. 1 XRD patterns for TS and SS of hot-pressed h-BN matrix composite ceramics with different YAG contents: (a) 10 wt%; (b) 20 wt%; (c) 30 wt%; and (d) 40 wt%.

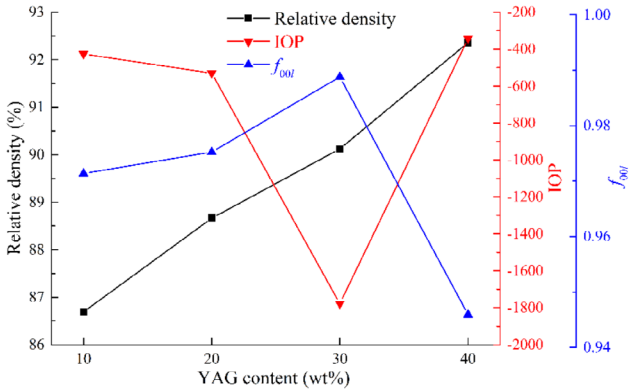

Fig. 2 Relative densities, IOP, and f_{00l} values of hot-pressed h-BN matrix composite ceramics with different YAG contents.

$$f_{00l} = \frac{P - P_0}{1 - P_0} \tag{2}$$

$$P \text{ and } P_0 = \frac{\sum I_{00l}}{\sum I_{hkl}} \tag{3}$$

where $\sum I_{00l}$ and $\sum I_{hkl}$ are the sums of the diffraction peak intensities of all (00*l*) and (*hkl*) planes, respectively. As (00*l*) planes are preferentially oriented on TS, P and P_0 are the ratio of $\sum I_{00l}$ to $\sum I_{hkl}$, among which P was calculated from the measured XRD patterns for TS of hot-pressed specimens, while P_0 was calculated from the standard JCPDS card (PDF#34-0421) of h-BN. P and f_{00l} are always lower than 1. A higher f_{00l} closer to 1 indicates more (00*l*) planes on TS.

When increasing the YAG content in hot-pressed h-BN matrix composite ceramics from 10 to 40 wt%, the absolute values of IOP and f_{00l} both increase first and then decrease dramatically, and reach the highest for BN-3YAG (IOP = −1778; f_{00l} = 0.99), which means that BN-3YAG has the highest texture degree.

Figure 3 shows the bright field images and selected area electron diffraction (SAED) patterns for SS of BN-3YAG and BN-4YAG. These plate-like h-BN grains are highly oriented with their (002) planes perpendicular to SS in BN-3YAG, which is confirmed by the SAED pattern of area A in Fig. 3(a). The SAED pattern of area B shows a secondary diffraction pattern caused by h-BN below the YAG area, and there are a row of diffraction spots deviating from the marked (002) direction, which was caused by the orientation difference of adjacent h-BN grains.

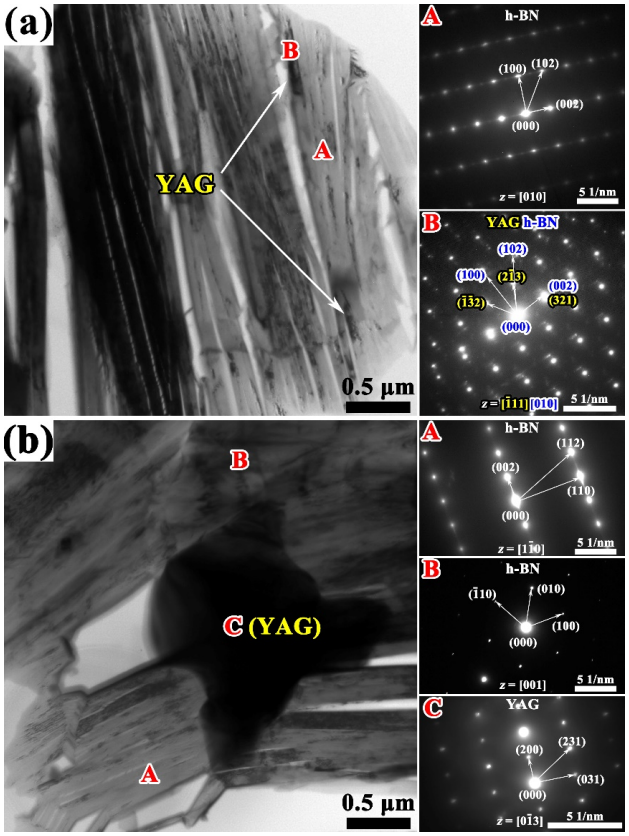

Fig. 3 Bright field images and SAED patterns for SS of (a) BN-3YAG and (b) BN-4YAG, respectively.

The arrangement of h-BN grains in BN-4YAG is not as orderly as that in BN-3YAG, which is demonstrated by the existence of both $(1\bar{1}0)$ planes (area A in Fig. 3(b)) and (002) planes (area B in Fig. 3(b)) of h-BN grains. The aggregation of liquid YAG phase formed during hot-pressing (area C in Fig. 3(b)) caused the buckling of plate-like h-BN grains, which significantly reduced the texture degree of BN-4YAG.

Figure 4 shows the high-resolution transmission electron microscopy (HRTEM) image, fast Fourier transform (FFT) pattens of several square regions in the HRTEM image, and corresponding inverse fast Fourier transformation (IFFT) images around the interface between h-BN and YAG in BN-3YAG. Areas 1–4 in Fig. 4(a) are h-BN, the interface between h-BN and YAG, YAG, and the h-BN area infiltrated by YAG, respectively. Stacking fault was observed in h-BN (Fig. 4(b)), which has been proven to commonly exist in hot-pressed h-BN ceramics due to the "multi-area co-growth" of h-BN grains in our previous study [29]. The IFFT image of area 2 in Fig. 4(a) displays the coherent interface between h-BN and YAG (Fig. 4(c)) formed due to the very close interplanar spacing between

the (002) plane of h-BN and the (100) plane of YAG, where the (002) and (100) planes of h-BN are parallel to the (321) and $(1\bar{4}5)$ planes of YAG, respectively. The IFFT image of area 3 in Fig. 4(a) displays the crystal structure of YAG observed from the $[\bar{1}11]$ direction (Fig. 4(d)), where the hexagons composed of Al and Y atoms can be easily distinguished, while the secondary diffraction pattern in the FFT pattern of area 3 confirms the existence of h-BN below the well-crystallized YAG area. The FFT pattern of area 4 indicates that this area contains both h-BN and YAG, and its IFFT image shows that the YAG phase infiltrates into the h-BN grain from multiple directions (Fig. 4(e)), further demonstrating the good wettability of YAG to h-BN grains.

Figure 5 shows the surface morphologies for TS and SS of hot-pressed h-BN matrix composite ceramics with different YAG contents. Many continuous small particles (< 0.5 μm) exist at the edges of plate-like h-BN grains, especially for BN-1YAG and BN-2YAG. Figure 6 shows the EDS spectra of points 1 and 2 in Fig. 5(d), where point 2 has much lower B and N peaks and much higher Y, Al, and O peaks compared with point 1, indicating that these small particles outside h-BN grains are YAG.

For BN-3YAG with the most highly textured microstructure, YAG particles were mainly observed on SS which contains most (100) planes, i.e., the side surfaces of plate-like h-BN grains. Such a result corresponds to the phenomenon that the diffraction peak intensities of YAG in the XRD patterns for SS are much higher than those for TS of BN-3YAG (Fig. 1(c)).

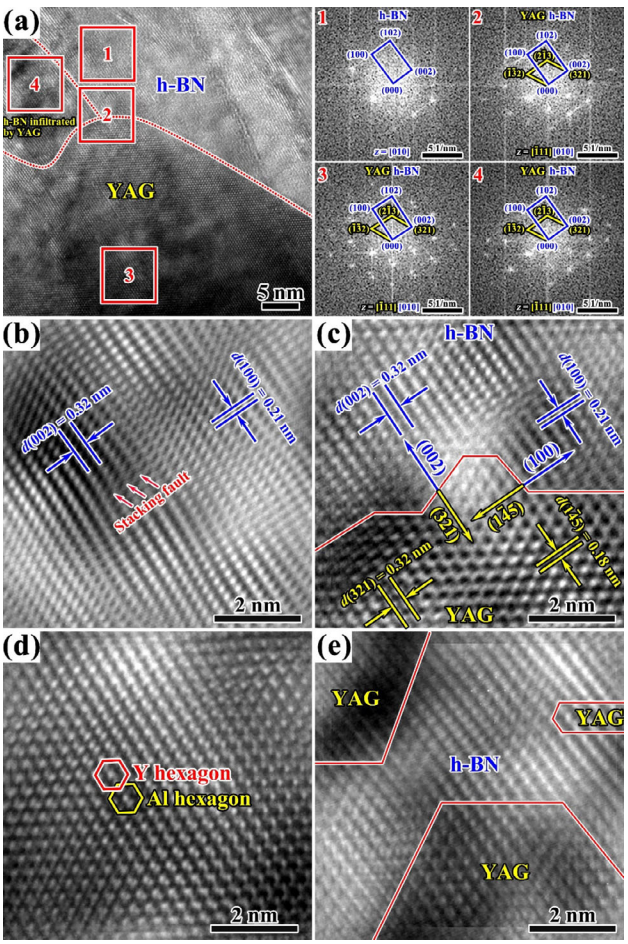

Fig. 4 Microstructure of the interface between h-BN and YAG in BN-3YAG: (a) HRTEM images and FFT patterns corresponding to areas 1–4, which are h-BN, the interface between h-BN and YAG, YAG, and the h-BN area infiltrated by YAG, respectively; (b–e) IFFT images corresponding to areas 1–4 in (a), respectively.

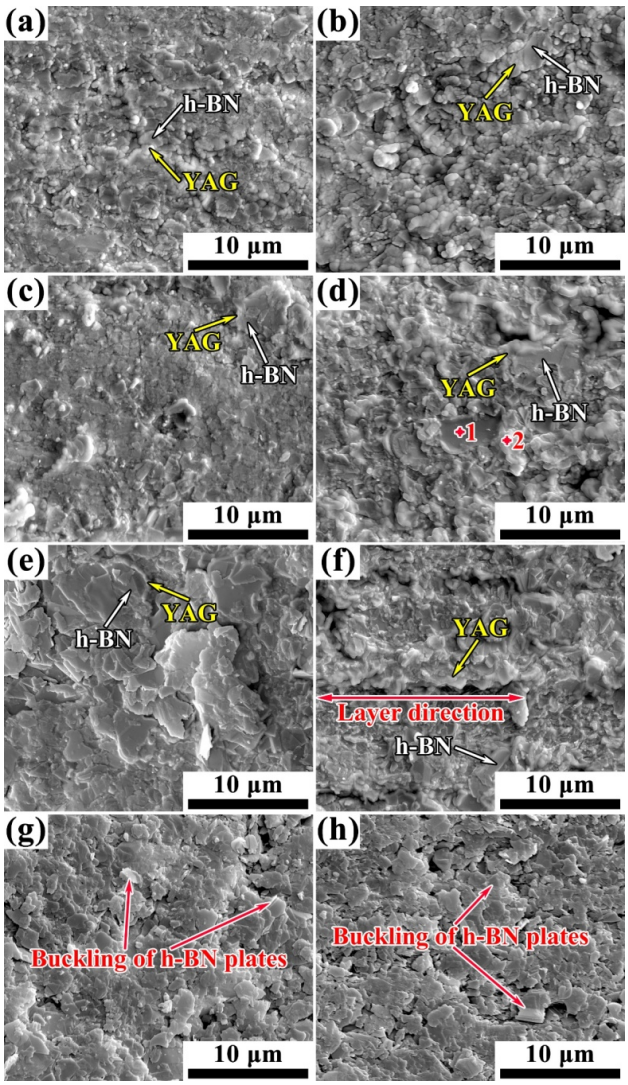

Fig. 5 Surface morphologies for (a, c, e, g) TS and (b, d, f, h) SS of hot-pressed h-BN matrix composite ceramics with different YAG contents: (a, b) BN-1YAG; (c, d) BN-2YAG; (e, f) BN-3YAG; and (g, h) BN-4YAG.

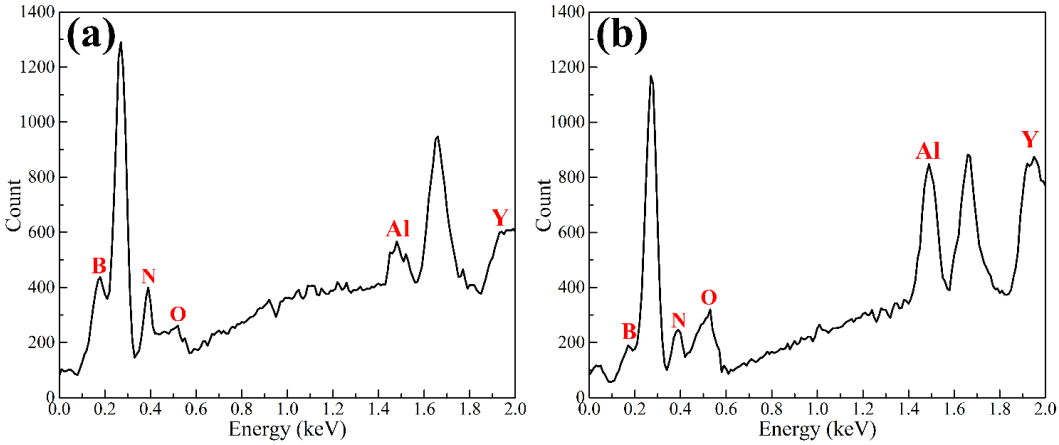

Fig. 6 EDS spectra of points (a) 1 and (b) 2 in Fig. 5(d).

For BN-4YAG, almost no YAG particles were observed, while many plate-like h-BN grains were buckled, which is consistent with the TEM observation in Fig. 3(b), indicating that YAG phase could be hidden under these buckled h-BN plates.

Figure 7(a) shows the schematic diagrams of the fracture modes and the fracture morphologies along different loading directions (D1, D2, and D3) of hot-pressed h-BN matrix composite ceramics with different YAG contents. For D1, the long axis of the sample bar is perpendicular to h-BN layers (parallel to the *c*-axis orientation) and the loading direction is parallel to h-BN layers, resulting in a relatively flat fracture morphology. For D2, the long axis of the sample bar is parallel to h-BN layers and the loading direction is perpendicular to h-BN layers, resulting in a tortuous crack propagation path. For D3, the long axis of the sample bar and the loading direction are both parallel to h-BN layers, generating a tortuous initial crack and a fracture morphology similar to that along D2.

The fracture morphologies of BN-3YAG show the most significant texture (Figs. 7(h)–7(j)), which is in consistent with its highest absolute values of IOP and f_{00l}. For BN-1YAG, the side of (002) plane of h-BN was observed on the fracture morphology along D1, and the (002) plane of h-BN was observed on the fracture morphology along D2 and D3 (Figs. 7(b)–7(d)). For BN-4YAG, many buckling behaviors of h-BN plates were observed (Figs. 7(k)–7(m)), which was caused by the aggregation of YAG phase (Fig. 3(b)) and significantly reduced its texture degree.

3. 2 Anisotropic properties

Figure 8 gives the mechanical properties of hot-pressed h-BN matrix composite ceramics with different YAG contents. The schematic diagram of samples with different orientations in the bulk specimen for testing anisotropy in mechanical properties was shown in Fig. 8(a). The work of fracture (γ_{WOF}) was calculated from the load–displacement curves during fracture toughness testing according to Eq. (4) [34]:

$$\gamma_{WOF} = \frac{\int F\mathrm{d}\delta}{2A} \tag{4}$$

where $\int F\mathrm{d}\delta$ is the total fracture energy during the fracture toughness testing which is determined as the area under the load–displacement curves, and A is the cross-sectional area of the unnotched part of the single-edge-notched beams.

As the sp^2 covalent bonds combining B and N atoms in the same atomic layer are much stronger than the vdW forces between different atomic layers, the mechanical properties along D1 of these hot-pressed h-BN matrix composite ceramics are much lower than those along D2 and D3. The elastic moduli, flexural strength, and fracture toughness along D3 of these specimens with different YAG contents are all a little higher than those along D2, which is attributed to the fact that the crack initiation along D2 only needs to break the sp^2 covalent bonds combining B and N atoms, while the crack initiation along D3 needs to break both the sp^2 covalent bonds combining B and N atoms and the vdW forces between different atomic layers.

If we considered the orientation of h-BN grains as the only factor influencing the mechanical properties, the increase of the texture degree would make it more difficult for the crack to initiate and propagate along

D2 and D3 as more sp^2 covalent bonds need to be broken, and make it easier for the crack to initiate and propagate along D1, resulting in higher mechanical properties along D2 and D3 and lower mechanical properties along D1. However, the YAG phase and relative density also have significant influence on the mechanical properties of these composite specimens. As YAG has a cubic crystal structure, it shows isotropic properties along different directions. Polycrystalline YAG ceramics were proven to show an elastic modulus around 300 GPa [35] and a flexural strength of 260–420 MPa [36], which are higher than the highest values of these h-BN matrix composite ceramics in this study. Therefore, the existence of YAG phase plays a role in strengthening and toughening along all loading directions of these composite specimens. Besides, a higher relative density, i.e., a lower porosity, also has a positive effect on the mechanical properties.

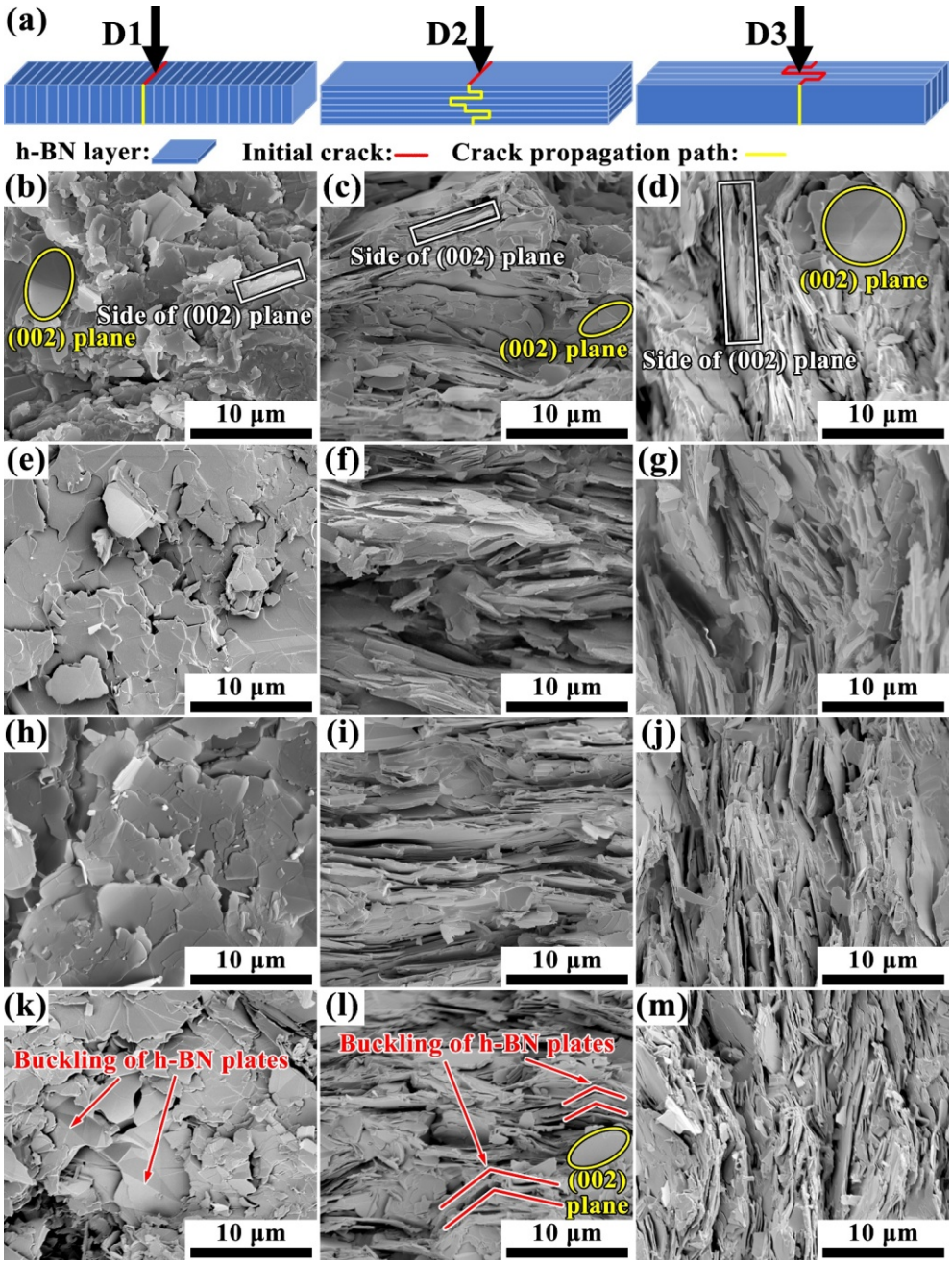

Fig. 7 Schematic diagrams of the fracture modes and fracture morphologies of hot-pressed h-BN matrix composite ceramics with different YAG contents: (a) schematic diagrams of the fracture modes along D1, D2, and D3; (b–d), (e–g), (h–j), and (k–m) show fracture morphologies along D1, D2, and D3 of BN-1YAG, BN-2YAG, BN-3YAG, and BN-4YAG, respectively.

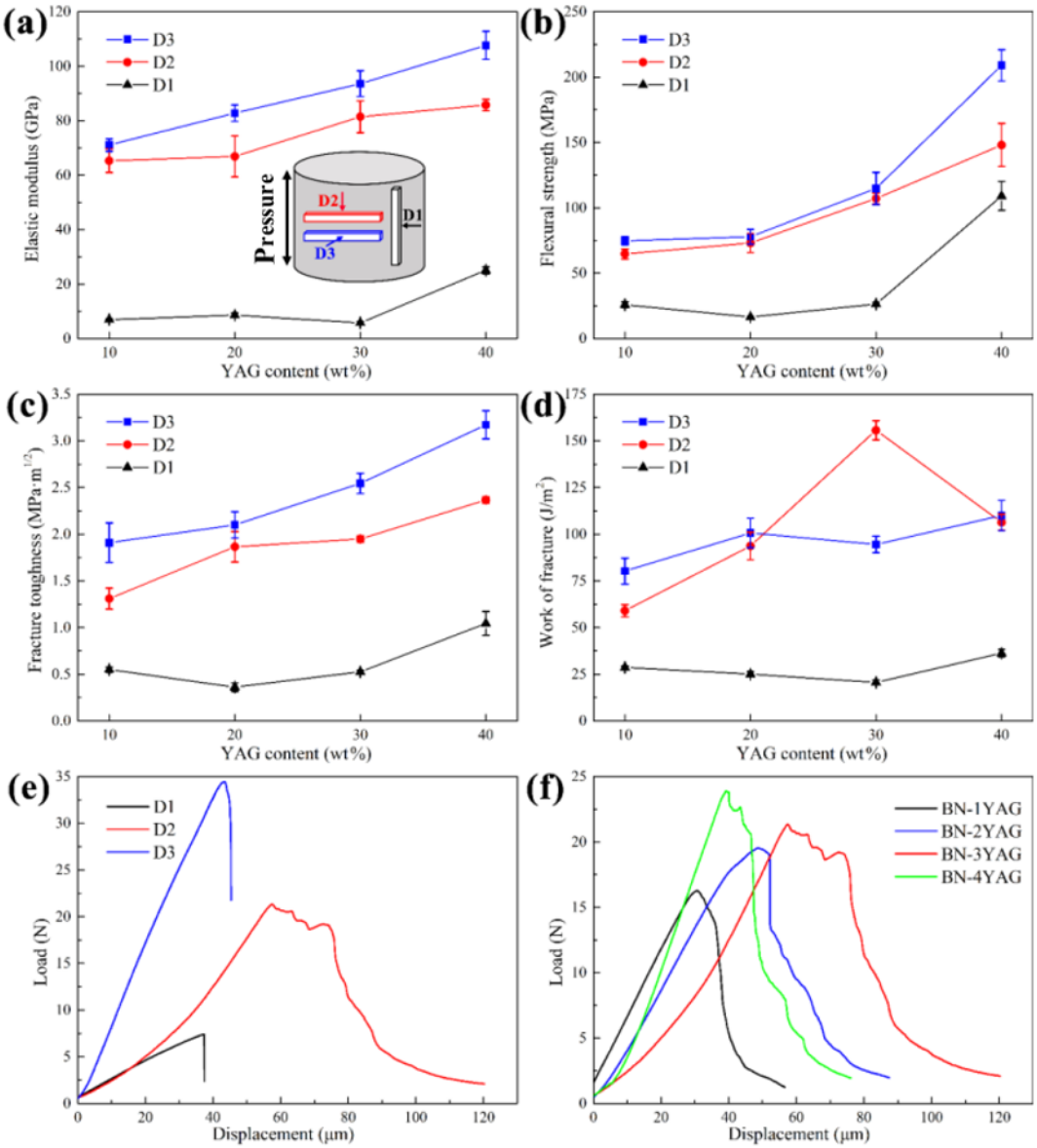

Fig. 8 Mechanical properties of hot-pressed h-BN matrix composite ceramics with different YAG contents: (a) elastic modulus; (b) flexural strength; (c) fracture toughness; (d) work of fracture; (e) load–displacement curves along D1, D2, and D3 of BN-3YAG; and (f) load–displacement curves along D2 of the specimens with different YAG contents.

As the YAG content increases from 10 to 30 wt%, the texture degree keeps increasing, which plays a role in strengthening and toughening along D2 and D3 and is harmful to the mechanical properties along D1, while the increased YAG content and relative density are beneficial to the mechanical properties along all loading directions. As a result, the elastic modulus, flexural strength, and fracture toughness along D1 show no significant change, while those along D2 and D3 keep increasing. As for BN-4YAG, although its texture degree drops dramatically compared with BN-3YAG, its higher relative density and YAG content give it the highest elastic modulus, flexural strength, and fracture toughness along all loading directions.

For h-BN matrix composite ceramics with the absolute value of IOP lower than 600 and f_{00l} lower than 0.98 (BN-1YAG, BN-2YAG, and BN-4YAG), their work of fracture along D2 is lower than that along D3, which is the same as the fracture toughness. However, for BN-3YAG with an IOP value of −1778 and a f_{00l} value as high as 0.99, its work of fracture along D2 (155.7± 5.1 J/m^2) is 66.7% higher than that along D3 (94.5± 4.5 J/m^2) and also 41.6% higher than the highest work of fracture (110.0±8.1 J/m^2) of other specimens despite

its lower fracture toughness along D2 than that along D3, which owes to its high texture degree and more tortuous crack propagation path along D2. Figure 8(e) shows the load–displacement curves along D1, D2, and D3 of BN-3YAG during the fracture toughness testing. The highest load along D3 is higher than that along D2, resulting in the higher fracture toughness along D3 than that along D2. BN-3YAG behaved a non-catastrophic fracture mode along D2 due to the orientation of plate-like h-BN grains, which resulted in step-by-step dropping of load with increasing the displacement during the tortuous crack propagation. Such a non-catastrophic fracture mode was also observed in the load–displacement curves along D2 of other specimens (Fig. 8(f)), where BN-3YAG behaved more significant step-by-step dropping of the load with the increase of the displacement, which is consistent with its high work of fracture and could improve its reliability in actual use as directional thermal conductive materials. Therefore, it could be speculated that a texture degree high enough (f_{00l} > 0.98) could significantly improve the work of fracture with the loading direction parallel to the *c*-axis orientation (D2) of h-BN matrix composite ceramics.

Figure 9 shows the lateral fracture morphologies along D2 of hot-pressed h-BN matrix composite ceramics with different YAG contents, where crack deflection phenomena correspond to the step-by-step dropping of load in Fig. 8(f). Different from BN-3YAG, the texture degrees of other specimens are not that high (f_{00l} < 0.98) to induce crack propagation paths tortuous enough which can give them higher work of fracture along D2 than that along D3.

Figure 10 shows the linear thermal expansion curves and CTE measured parallel and perpendicular to the *c*-axis orientation of hot-pressed h-BN matrix composite ceramics with different YAG contents. The schematic diagram of samples with different orientations in the bulk specimen for testing anisotropy in thermal expansion is shown in Fig. 10(b). The CTE of YAG was calculated to be 7×10^{-6} K^{-1} at room temperature based on the lattice parameters obtained from XRD [37]. The CTE perpendicular to the *c*-axis of h-BN is -2.72×10^{-6} K^{-1} at room temperature and approaches zero at high temperatures, while the CTE parallel to the *c*-axis of h-BN is 37.7×10^{-6} K^{-1} at room temperature and tends to be invariable at high temperatures [38].

A higher texture degree tends to decrease the CTE perpendicular to the *c*-axis orientation and increase that parallel to the *c*-axis orientation, while a higher YAG content tends to increase the CTE perpendicular to the *c*-axis orientation and decrease that parallel to the *c*-axis orientation. A higher relative density tends to decrease the CTE along both directions. As a result, the CTE perpendicular to the *c*-axis orientation keeps increasing with the increase of YAG content due to the contribution of YAG, while that parallel to the *c*-axis orientation first decreases from 10 wt% YAG to 20 wt% YAG attributed to the increased YAG content and relative density and then increases from 20 wt% YAG to 30 wt% YAG due to the increased texture degree. With the further increase of the YAG content to 40 wt%, the CTE parallel to the *c*-axis orientation decreases drastically due to the increased YAG content and relative density and the decreased texture degree.

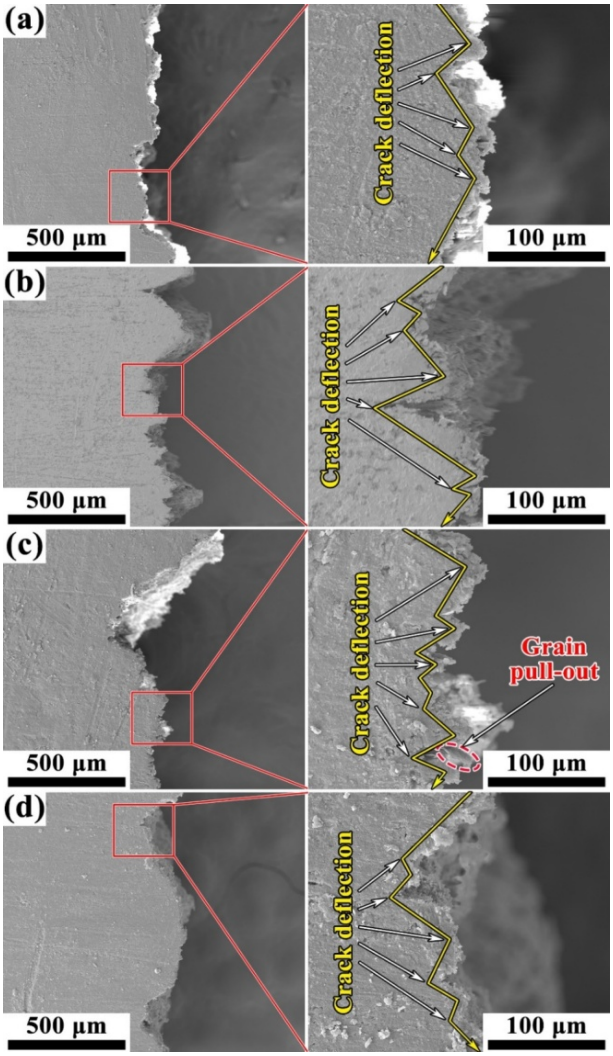

Fig. 9 Lateral fracture morphologies along D2 of hot-pressed h-BN matrix composite ceramics with different YAG contents: (a) BN-1YAG; (b) BN-2YAG; (c) BN-3YAG; and (d) BN-4YAG.

Figure 11 gives the specific heat, thermal diffusivity, and thermal conductivity (25–1200 ℃) parallel and perpendicular to the *c*-axis orientation of hot-pressed h-BN matrix composite ceramics with different YAG contents and their anisotropy degrees in thermal conductivity, which were determined by the ratio of the thermal conductivity perpendicular to the *c*-axis orientation to that parallel to the *c*-axis orientation. The schematic diagram of samples with different orientations in the bulk specimen for testing anisotropy in thermal conductivity is shown in Fig. 11(b). The specific heat at room temperature of YAG was measured to be around 0.6 J/(K·g) by the differential scanning calorimeter [39], which was lower than 0.8 J/(K·g) of h-BN [40]. As a result, the specific heat of these composite specimens decreases with the increase of YAG content. Besides, all specimens have higher specific heat at higher temperatures.

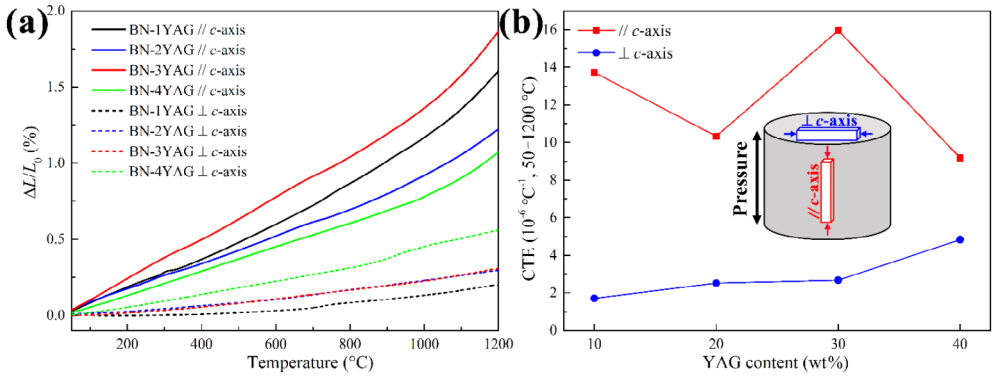

Fig. 10 (a) Linear thermal expansion curves and (b) CTEs measured parallel and perpendicular to the *c*-axis orientation of hot-pressed h-BN matrix composite ceramics with different YAG contents.

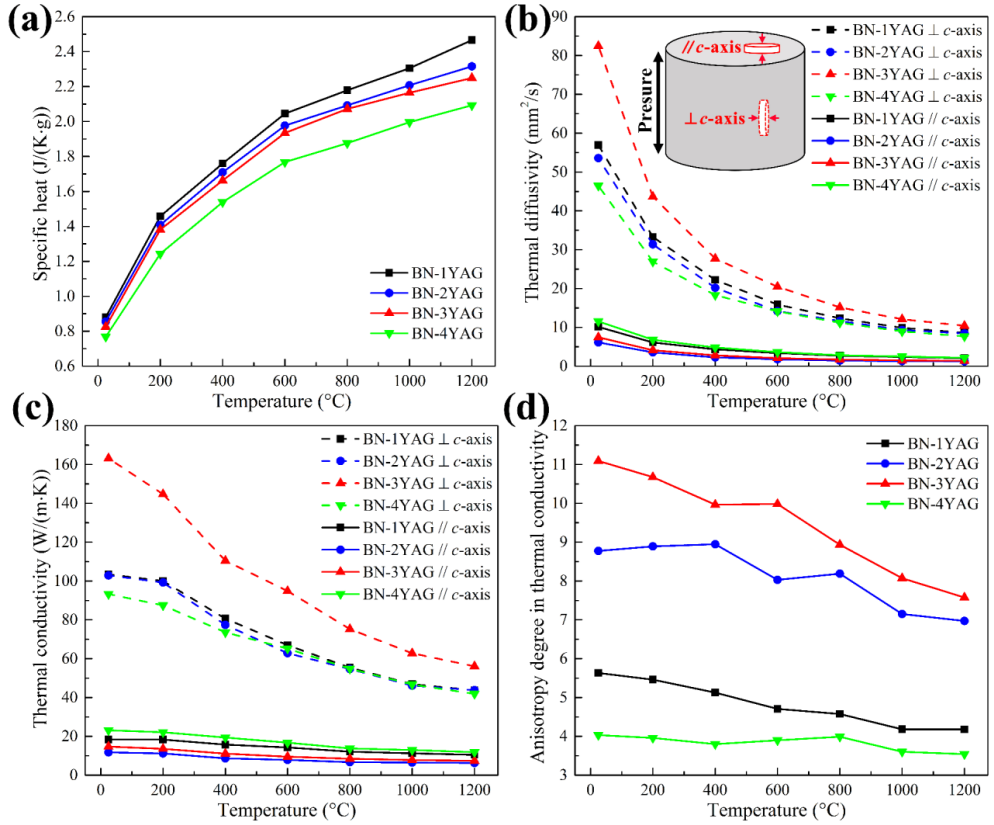

Fig. 11 (a) Specific heat, (b) thermal diffusivity, and (c) thermal conductivity parallel and perpendicular to the *c*-axis orientation; and (d) anisotropy degrees in thermal conductivity of hot-pressed h-BN matrix composite ceramics with different YAG contents.

The thermal diffusivity and thermal conductivity perpendicular to the *c*-axis orientation are higher than those parallel to the *c*-axis orientation of these composite specimens due to the anisotropic thermal conductivity of h-BN [8]. A higher texture degree would result in higher thermal conductivity perpendicular to the *c*-axis orientation and lower thermal conductivity parallel to the *c*-axis orientation. Although the thermal conductivity of YAG was measured to be only −10 W/(m·K) at room temperature [39], BN-3YAG, which has the highest texture degree, still has the highest thermal diffusivity (82.4 mm^2/s at 25 ℃) and thermal conductivity (163.2 W/(m·K) at 25 ℃) perpendicular to the *c*-axis orientation, which are 11.1 times those (7.4 mm^2/s and 14.7 W/(m·K), respectively) parallel to the *c*-axis orientation at room temperature. However, the higher relative density of BN-3YAG gives it higher thermal conductivity parallel to the *c*-axis orientation than that of BN-2YAG (11.7 W/ (m·K) at 25 ℃), and the higher YAG content of BN- 2YAG (102.9 W/(m·K) at 25 ℃) gives it lower thermal conductivity perpendicular to the *c*-axis orientation than that of BN-1YAG (103.4 W/(m·K) at 25 ℃), although the former has a higher texture degree than the latter.

The thermal diffusivity and thermal conductivity of these composite ceramics decrease and the decrease rate gets slower with the increase of the testing temperature (Figs. 11(a) and 11(b)), especially for those parallel to the *c*-axis orientation, which is attributed to the influence of temperature on the mean free path of phonons. As the thermal conduction in h-BN is achieved by phonon transport, the thermal conductivity of h-BN matrix composite ceramics can be evaluated by Eq. (5) [41,42]:

$$k=\frac{1}{3}Cvl \tag{5}$$

where k is the thermal conductivity achieved by phonon transport, C is the specific heat which increases with the increase of the temperature, v is the velocity of phonons which is influenced by the grain orientation, and l is the mean free path of phonons which is influenced by both the temperature and grain size.

With increasing the testing temperature from room temperature, the number of phonons increases dramatically, which causes more scattering phenomena between phonons and phonons, leading to the decrease of l. Further increase of temperature diminishes l to be closer to the lattice spacing, and thus the adverse effect of temperature on the thermal conductivity decreases; meanwhile, the specific heat increases, making thermal conductivity tends to be constant. For the thermal conduction parallel to the *c*-axis orientation, the grain size (the thickness of plate-like h-BN grains) is very small, and thus there exist many phonon scattering phenomena caused by grain boundaries, that is, many phonons get scattered by grain boundaries before encountering other phonons. Therefore, the decrease rate of the thermal conductivity parallel to the *c*-axis orientation is slower than that perpendicular to the *c*-axis orientation, leading to the decrease of the anisotropy degree in the thermal conductivity with the increase the testing temperature, especially for BN-3YAG having the highest texture degree (Fig. 11(c)).

4 Conclusions

Textured h-BN matrix composite ceramics with different contents of YAG formed *in situ* from the $3Y_2O_3$–$5Al_2O_3$ sintering additive were fabricated by hot-pressing. The YAG phase shows good wettability to h-BN grains, and a coherent relationship between h-BN and YAG was observed with $[010]_{h\text{-}BN}//[\bar{1}11]_{YAG}$ and $(002)_{h\text{-}BN}//(321)_{YAG}$. The rotation of plate-like h-BN grains under the uniaxial pressure in the liquid YAG phase during hot-pressing led to textured microstructures with the *c*-axis of h-BN grains preferentially oriented parallel to the sintering pressure direction, giving these composite ceramics anisotropy in their mechanical and thermal properties. They show better mechanical properties along D2 and D3 than those along D1, higher coefficients of thermal expansion parallel to the *c*-axis orientation than those perpendicular to the *c*-axis orientation, and higher thermal conductivity perpendicular to the *c*-axis orientation than that parallel to the *c*-axis orientation.

With increasing the YAG content, the texture degree of the composite specimen first increases, reaching the highest with a f_{00l} of 0.99 for the specimen with 30 wt% YAG. Further increase of the YAG content (40 wt%) resulted in the aggregation of liquid YAG phase which caused the buckling of h-BN plates and significantly reduced the texture degree. The anisotropy degrees in mechanical and thermal properties of these composite specimens are not totally consistent with their texture degrees due to their different YAG contents and relative density.

Textured h-BN matrix composite ceramics behave a non-catastrophic fracture mode when the crack propagates through h-BN layers, among which the

specimen with 30 wt% YAG has the highest work of fracture (155.7±5.1 J/m^2) due to its highest texture degree, which also has the highest anisotropy degree in thermal conductivity (14.7 and 163.2 W/(m·K) parallel and perpendicular to the *c*-axis orientation at 25 ℃, respectively), making it a promising candidate as thermal management devices in electronics.

Acknowledgements

This work was supported by the National Natural Science Foundation of China (Nos. 52072089, 51832002, 51602074, and 51672060) and the Heilongjiang Touyan Team Program.

References

[1] Song L, Ci L, Lu H, *et al*. Large scale growth and characterization of atomic hexagonal boron nitride layers. *Nano Lett* 2010, **10**: 3209–3215.

[2] Li Y, Ge B, Wu Z, *et al*. Effects of h-BN on mechanical properties of reaction bonded β-SiAlON/h-BN composites. *J Alloys Compd* 2017, **703**: 180–187.

[3] Jin H, Li Y, Li X, *et al*. Functionalization of hexagonal boron nitride in large scale by a low-temperature oxidation route. *Mater Lett* 2016, **175**: 244–247.

[4] Tian Z, Chen K, Sun S, *et al*. Crystalline boron nitride nanosheets by sonication-assisted hydrothermal exfoliation. *J Adv Ceram* 2019, **8**: 72–78.

[5] Xiao L, He WJ, Yin YS. First-principles calculations of structural and elastic properties of hexagonal boron nitride. *Adv Mater Res* 2009, **79–82**: 1337–1340.

[6] Zhang Z, Duan X, Qiu B, *et al*. Preparation and anisotropic properties of textured structural ceramics: A review. *J Adv Ceram* 2019, **8**: 289–332.

[7] Duan X, Wang M, Jia D, *et al*. Anisotropic mechanical properties and fracture mechanisms of textured h-BN composite ceramics. *Mater Sci Eng A* 2014, **607**: 38–43.

[8] Jiang P, Qian X, Yang R, *et al*. Anisotropic thermal transport in bulk hexagonal boron nitride. *Phys Rev Materials* 2018, **2**: 064005.

[9] Yan W, Zhang Y, Sun H, *et al*. Polyimide nanocomposites with boron nitride-coated multi-walled carbon nanotubes for enhanced thermal conductivity and electrical insulation. *J Mater Chem A* 2014, **2**: 20958–20965.

[10] Eichler J, Lesniak C. Boron nitride (BN) and BN composites for high-temperature applications. *J Eur Ceram Soc* 2008, **28**: 1105–1109.

[11] Fang H, Bai SL, Wong CP. "White graphene"-hexagonal boron nitride based polymeric composites and their application in thermal management. *Compos Commun* 2016, **2**: 19–24.

[12] Meziani MJ, Song WL, Wang P, *et al*. Boron nitride nanomaterials for thermal management applications. *ChemPhysChem* 2015, **16**: 1339–1346.

[13] Li X, Long Y, Ma L, *et al*. Coating performance of hexagonal boron nitride and graphene layers. *2D Mater* 2021, **8**: 034002.

[14] Zhang Z, Hu S, Chen J, *et al*. Hexagonal boron nitride: A promising substrate for graphene with high heat dissipation. *Nanotechnology* 2017, **28**: 225704.

[15] Zhu Z, Wang P, Lv P, *et al*. Densely packed polymer/boron nitride composite for superior anisotropic thermal conductivity. *Polym Compos* 2018, **39**: E1653–E1658.

[16] Wilk A, Rutkowski P, Zientara D, *et al*. Aluminium oxynitride-hexagonal boron nitride composites with anisotropic properties. *J Eur Ceram Soc* 2016, **36**: 2087–2092.

[17] Shi Z, Wang J, Qiao G, *et al*. Effects of weak boundary phases (WBP) on the microstructure and mechanical properties of pressureless sintered Al_2O_3/h-BN machinable composites. *Mater Sci Eng A* 2008, **492**: 29–34.

[18] Jin H, Shi Z, Li X, *et al*. Effect of rare earth oxides on the microstructure and properties of mullite/hBN composites. *Ceram Int* 2017, **43**: 3356–3362.

[19] Liu Z, Zhao S, Yang T, *et al*. Improvement in mechanical properties in AlN-h-BN composites with high thermal conductivity. *J Adv Ceram* 2021, **10**: 1317–1325.

[20] Chen J, Chen J. Formation and thermal stability of dual glass phases in the h-BN/SiO_2/Yb–Si–Al–O composites. *J Eur Ceram Soc* 2020, **40**: 456–462.

[21] Chen J, Chen J, Zhang X, *et al*. Fabrication and mechanical properties of h-BN based composites containing dual glass phases. *J Eur Ceram Soc* 2018, **38**: 3210–3216.

[22] Zhang Z, Duan X, Qiu B, *et al*. Anisotropic properties of textured h-BN matrix ceramics prepared using $3Y_2O_3$–$5Al_2O_3$(–4MgO) as sintering additives. *J Eur Ceram Soc* 2019, **39**: 1788–1795.

[23] Zhang X, Chen J, Li X, *et al*. Microstructure and mechanical properties of h-BN/Y_2SiO_5 composites. *Ceram Int* 2015, **41**: 1279–1283.

[24] Kusunose T, Sekino T. Thermal conductivity of hot-pressed hexagonal boron nitride. *Scripta Mater* 2016, **124**: 138–141.

[25] Chen J, Chen J, Zhang H, *et al*. Microstructure and mechanical properties of h-BN/$Yb_4Si_2O_7N_2$ composites. *J Adv Ceram* 2018, **7**: 317–324.

[26] Qiu B, Duan X, Zhang Z, *et al*. Microstructural evolution of h-BN matrix composite ceramics with La–Al–Si–O glass phase during hot-pressed sintering. *J Adv Ceram* 2021, **10**: 493–501.

[27] Ni DW, Zhang GJ, Kan YM, *et al*. Textured h-BN ceramics prepared by slip casting. *J Am Ceram Soc* 2011, **94**: 1397–1404.

[28] Xue JX, Liu JX, Xie BH, *et al*. Pressure-induced preferential grain growth, texture development and anisotropic properties of hot pressed hexagonal boron nitride ceramics. *Scripta Mater* 2011, **65**: 966–969.

[29] Zhang Z, Duan X, Qiu B, *et al*. Microstructure evolution and grain growth mechanisms of h-BN ceramics during

hot-pressing. *J Eur Ceram Soc* 2020, **40**: 2268–2278.
[30] Duan X, Jia D, Wang Z, *et al*. Influence of hot-press sintering parameters on microstructures and mechanical properties of h-BN ceramics. *J Alloys Compd* 2016, **684**: 474–480.
[31] Zhang Z, Duan X, Qiu B, *et al*. Improvement of grain size and crystallization degree of LPSed h-BN composite ceramics by amorphization/nanocrystallization of raw h-BN powders. *J Alloys Compd* 2021, **852**: 156765.
[32] Hubäĉek M, Ueki M, Satό T. Orientation and growth of grains in copper-activated hot-pressed hexagonal boron nitride. *J Am Ceram Soc* 1996, **79**: 283–285.
[33] Lotgering FK. Topotactical reactions with ferrimagnetic oxides having hexagonal crystal structures-I. *J Inorg Nucl Chem* 1959, **9**: 113–123.
[34] Pavlacka R, Bermejo R, Chang Y, *et al*. Fracture behavior of layered alumina microstructural composites with highly textured layers. *J Am Ceram Soc* 2013, **96**: 1577–1585.
[35] Yagi H, Yanagitani T, Numazawa T, *et al*. The physical properties of transparent $Y_3Al_5O_{12}$: Elastic modulus at high temperature and thermal conductivity at low temperature. *Ceram Int* 2007, **33**: 711–714.
[36] Tong H, Wang N, Zou Y, *et al*. Densification and mechanical properties of YAG ceramics fabricated by air pressureless sintering. *J Electron Mater* 2019, **48**: 374–385.
[37] Klein PH, Croft WJ. Thermal conductivity, diffusivity, and expansion of Y_2O_3, $Y_3Al_5O_{12}$, and LaF_3 in the range 77°–300°K. *J Appl Phys* 1967, **38**: 1603–1607.
[38] Paszkowicz W, Pelka JB, Knapp M, *et al*. Lattice parameters and anisotropic thermal expansion of hexagonal boron nitride in the 10–297.5 K temperature range. *Appl Phys A* 2002, **75**: 431–435.
[39] Sato Y, Taira T. The studies of thermal conductivity in GdVO(4), YVO(4), and Y(3)Al(5)O(12) measured by quasi-one-dimensional flash method. *Opt Express* 2006, **14**: 10528–10536.
[40] Gavrichev KS, Solozhenko VL, Gorbunov VE, *et al*. Low-temperature heat capacity and thermodynamic properties of four boron nitride modifications. *Thermochimica Acta* 1993, **217**: 77–89.
[41] Slack GA, Tanzilli RA, Pohl RO, *et al*. The intrinsic thermal conductivity of AIN. *J Phys Chem Solids* 1987, **48**: 641–647.
[42] Watari K, Ishizaki K, Fujikawa T. Thermal conduction mechanism of aluminium nitride ceramics. *J Mater Sci* 1992, **27**: 2627–2630.